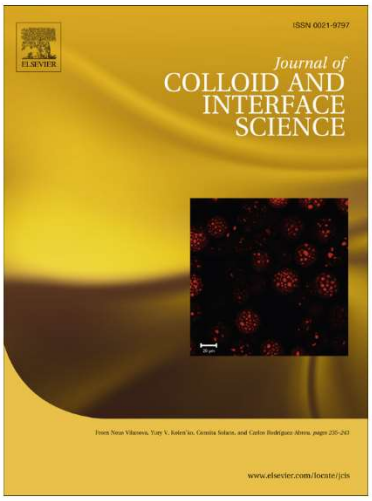

Size and Morphology Dependent Surface Wetting Based on Hydrocarbon Functionalized Nanoparticles

Donald Hill, Hadi Attia, Andrew R. Barron, Shirin Alexander

PII: S0021-9797(19)30232-2
DOI: https://doi.org/10.1016/j.jcis.2019.02.058
Reference: YJCIS 24682

To appear in: *Journal of Colloid and Interface Science*

Received Date: 20 November 2018
Revised Date: 18 February 2019
Accepted Date: 19 February 2019

Please cite this article as: D. Hill, H. Attia, A.R. Barron, S. Alexander, Size and Morphology Dependent Surface Wetting Based on Hydrocarbon Functionalized Nanoparticles, *Journal of Colloid and Interface Science* (2019), doi: https://doi.org/10.1016/j.jcis.2019.02.058

Size and Morphology Dependent Surface Wetting Based on Hydrocarbon Functionalized Nanoparticles

Donald Hill[a], Hadi Attia[b,c], Andrew R. Barron[a,d,e], Shirin Alexander[*a]

[a] Energy Safety Research Institute (ESRI), Swansea University Bay Campus, Fabian Way, Swansea SA1 8EN, UK.

[b] Centre for Water Advanced Technologies and Environmental Research (CWATER), College of Engineering, Swansea University, Fabian Way, Swansea SA1 8EN, UK.

[c] Environmental Engineering Department, Al-Mustansiriya University, Iraq

[d] Department of Chemistry, Rice University, Houston, TX 77005, USA.

[e] Department of Materials Science and Nanoengineering, Rice University, Houston, Texas 77005, USA.

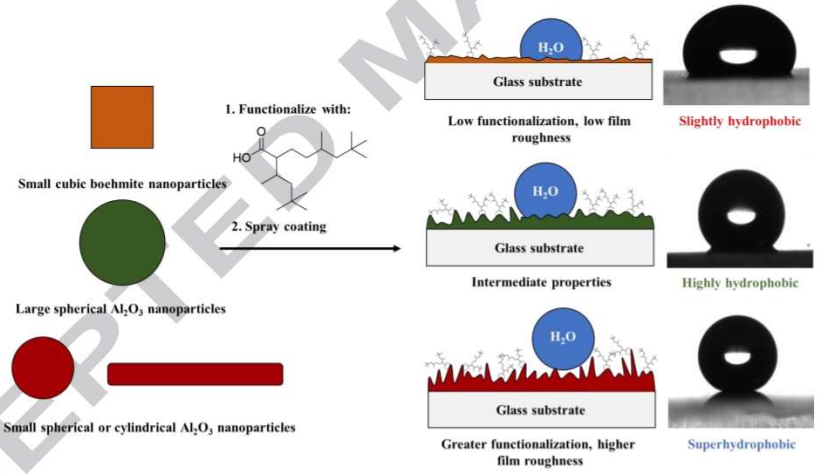

* Corresponding author. Tel.: +44 (0)1792 606230.

E-mail addresses: s.alexander@swansea.ac.uk

ABSTRACT:

Hypothesis: The wetting properties of films created using metal oxide nanoparticles can be controlled through roughness and chemical functionality; however, other variations such as the size and shape of the particles play an important role in improved understanding of the wetting behaviour of these materials.

Experiments: Infrared (IR) spectroscopy and thermogravimetric analysis (TGA) were used to study the chemisorption and grafting density of a carboxylic acid onto the surface of nanoparticles. Scanning electron microscopy (SEM) and atomic force microscopy (AFM) were used to investigate the morphology and roughness of the nanoparticle films. To investigate the wettability and surface energy of the films, static and dynamic contact angle (CA) measurements were used.

Findings: Smaller, spherical nanoparticles (<50 nm) were observed to create films that displayed greater surface roughness and showed superhydrophobic properties. By comparison, larger, 135 nm spherical nanoparticles showed reduced surface roughness and displayed water contact angles (WCAs) <150°. Since these particles showed similar carboxylate grafting densities, this suggests that there is a particle size limit above which it is not possible to deposit superhydrophobic films. This study also shows that topographical effects brought about by film roughness can be overcome through increasing the carboxylate grafting density on the surface of the nanoparticles. It was observed that films created using mix shape <50 nm nanoparticles with relatively low surface roughness displayed superhydrophobic WCAs and low hysteresis. These particles also possessed a substantially larger carboxylate grafting density, indicating that the extent of functionalization also has a large bearing on the wettability of the films. Herein, we show that particle size, morphology, and reactivity all play important roles in determining the wettability of nanoparticle films.

Keywords: Surface modification, Superhydrophobic Nanoparticles, Particle size, Hydrocarbon Low Surface Energy Materials (LSEMs).

1. Introduction

Coatings formed from functionalized nanoparticles have been reported to imbue a variety of materials with superhydrophobic properties [1-3]. Functionalization of nanoparticles with low surface energy compounds offers an attractive method of synthesising superhydrophobic materials since the particles are often commercially available and relatively cheap. Furthermore, this methodology is also appealing since the nanoparticles can be readily

applied to different surfaces through versatile coating techniques such as dip [2] or spray coating [3]. Metal oxide nanoparticles, such as ZnO [2,4], Al_2O_3 [3] or Fe_3O_4 [2,5], have been widely used in these studies, and have been functionalised with low surface energy compounds such as carboxylic acids [3,4,6] and organosilanes [1,2,5].

It has been shown that dual micro- and nanoscale surface roughness is required for surfaces to show superhydrophobicity [7,8]. This is because the grooves created by the surface roughness are believed to trap pockets of air, resulting in a state where water droplets do not penetrate between the grooves and readily roll off the surfaces [8,9]. It has been observed that coatings formed from functionalized nanoparticles possess rough surface morphologies that are able to suspend water droplets from spreading [3,4,5]. Generation of surface roughness using nanoparticle films is an attractive alternative to techniques that alter the physical form of materials in order to achieve the desired surface texture. Techniques that remove material from surfaces such as etching [10,11], laser ablation [12,13], and ion bombardment [14,15] have been shown to create surface roughness that is necessary for superhydrophobicity. However, these methods permanently alter the physical form of substrates, which can make them less suitable for use in the desired applications (such as self-cleaning and water resistance food packaging, water-proof textiles, papers, and fibres and anti-corrosion metal coatings).

Coatings formed from hydrophobic nanoparticles do not rely on the underlying surface texture of the substrate in order to display superhydrophobicity. The majority of studies reporting superhydrophobic nanoparticle films have used particles of one size to create the desired level of surface roughness [1-6]. However, some studies have investigated using nanoparticles of different sizes to create surface textures more representative of natural superhydrophobic surfaces [16,17]. Studies using modified SiO_2 nanoparticles have shown that coatings prepared using smaller particles are more hydrophobic [16,18]. These coatings showed rougher morphologies [16], enabling them to trap more air between the surface features and thus display higher contact angles [19].

Although the influence of particle size on wettability has been studied previously [16,18], to our knowledge, no studies have been reported that discuss how particle morphology affects the wetting properties of nanoparticle films. In addition, existing reports that compare nanoparticle films have not studied how the number of chemisorbed molecules on the surface of the particles affects the wettability.

In our previous works we showed for the first time that environmentally friendly, non-hazardous and cost effective superhydrophobic nanoparticles could be formed using

hyperbranched hydrocarbons rather than fluorocarbons and polymers [3,6]. Herein the effect of nanoparticles shape, size and reactivity on the wetting properties of films is investigated. The films were formed using five different types of commercially available nanoparticles and highly branched hydrocarbon, isostearic acid was used for surface functionalization, using a method described in our previous work [3]. The nanoparticles used here are either Al_2O_3 or boehmite (γ-AlO(OH)).

2. Materials and methods

2.1 Materials

Toluene (≥99.5%), isopropanol (≥99.7%) and ethanol absolute (≥99.8%) were purchased from Sigma-Aldrich and VWR Chemicals. Isostearic acid was provided by Nissan Chemical Industries and used without further purification. Distilled water (Millipore, 18 MΩ cm) was used during the WCA measurements. The 5 nm cubic pseudo boehmite nanoparticles (Pural SB 74% Al_2O_3) were provided by Sasol Performance Chemicals and the < 50 nm Al_2O_3 nanoparticles were purchased from Sigma-Aldrich. The other Al_2O_3 nanoparticles (99.9%) were purchased from US Research Nanomaterials, Inc. Microscope slides were purchased from VWR Chemicals. Images showing the different particle morphologies taken from the manufacturers are shown in Figure S1.

2.2. Methods

2.2.1. Synthesis of the isostearic functionalized nanoparticles and preparation of the nanoparticle films

Synthesis of the isostearic functionalized nanoparticles was performed in a similar manner to described previously [3]. The Al_2O_3 nanoparticles were refluxed with isostearic acid in toluene in a 1:1.5 molar ratio. Functionalization of the boehmite nanoparticles was achieved using 1:2.8 molar ratio of boehmite to isostearic acid. This was performed because of the higher surface area of the boehmite nanoparticles (Table 1). Typically, 5.0 g of nanoparticles were refluxed in 100 mL of toluene for at least 12 hours, along with the appropriate amount of isostearic acid (20.9 g Al_2O_3 nanoparticles or 71.3 g of boehmite nanoparticles). Once the reaction time had elapsed, the mixtures were centrifuged at 5000 rpm for 30 minutes. The supernatant was decanted and the nanoparticles centrifuged twice in isopropanol and once in ethanol. The nanoparticle slurries were then oven-dried at 80 °C for

at least 12 hours. Nanoparticle films were spray-coated onto glass microscope slides at 80 °C from 2 %wt suspensions in isopropanol.

2.2.2. Characterization methods

Scanning electron microscopy (SEM) was performed using a Hitachi Field Emission S-4800 scanning microscope. Atomic force microscopy (AFM) was carried out using a JPK Nanowizard AFM in non-contact mode. Surface roughness values for the films were measured from three different 10 × 10 μm^2 areas of the surfaces. Values of the surface roughness parameters discussed in this paper are the average of these three measurements, uncertainties are the standard deviation from the mean. Thermogravimetric analysis (TGA) was conducted using a TA Instrument SDT Q600 under static air-flow. Nanoparticles were loaded into an open alumina crucible during the measurements and heated from 50 to 800 °C at a rate of 20 °C min^{-1}. Infrared (IR) spectroscopy was carried out using a Thermoscientific i510 in the range of 400 - 4000 cm^{-1}. Typically 16 scans were performed during each measurement. Contact angle measurements (static contact angle, advancing and receding contact angle) were obtained using the sessile drop method and were carried out using a DSA25 Expert Drop Shape Analyzer (Krüss). Measurements were performed under ambient conditions using deionized water. Diiodomethane was also used for surface free energy (SFE) measurements. SFE measurements were calculated using Krüss software and the OWRK model [20]. Each stated contact angle is the average of three measurements from various positions on the surface. Uncertainties associated with the contact angles were also calculated using Krüss software.

3. Results and discussion

Films were prepared through spray coating onto glass microscope slides. Table 1 shows some of the properties of the as received nanoparticles, and the contact angles of the films created using these nanoparticles on glass microscope slides. As shown in Table 1, the particles possess a wide range of surface areas, and the non-functionalized films are hydro- and oleophilic before functionalization with isostearic acid.

Table 1

Water (WCA) and diiodomethane (CA) contact angles of the as received nanoparticles spray-coated onto glass microscope slides. Particle sizes, surface areas and morphological information were supplied by the manufacturers.

Type	Size (nm)	Surface area (m^2/g)	Morphology	WCA (°)	CH_2I_2 CA(°)	SFE (mN/m)
Al_2O_3	5	150	Spherical	10 ±3	6±1	80±1
Al_2O_3	50	35	Spherical	17 ±1	9±1	78±1
Al_2O_3	135	18-25	Spherical	53 ±7	10±1	59±5
Al_2O_3	<50	40	Mix shape- mainly cylindrical	<5	<5	-
γ-AlO(OH)	5	250	Cubic/ hexagonal crystals	<5	7±1	-

3.1. Surface functionalization and carboxylate loading

Prior to functionalization, the IR spectra of the as received nanoparticles show no significant bands except -OH stretching modes at the region of 3301 to 3464 cm^{-1} [21] (Fig. 1a). Following modification with isostearic acid, all of the nanoparticles show CH_2/CH_3 stretching bands between 2963 and 2929 cm^{-1} due to the aliphatic stretches of the acid. Symmetric stretches at 1468 cm^{-1} and asymmetric stretches at about 1556 cm^{-1} are due to carbonyls in bidentate modes, indicating an occurrence of the chemical reaction between the carboxylic acid and the -OH groups of the nanoparticles (Fig. 1b) [22-24].

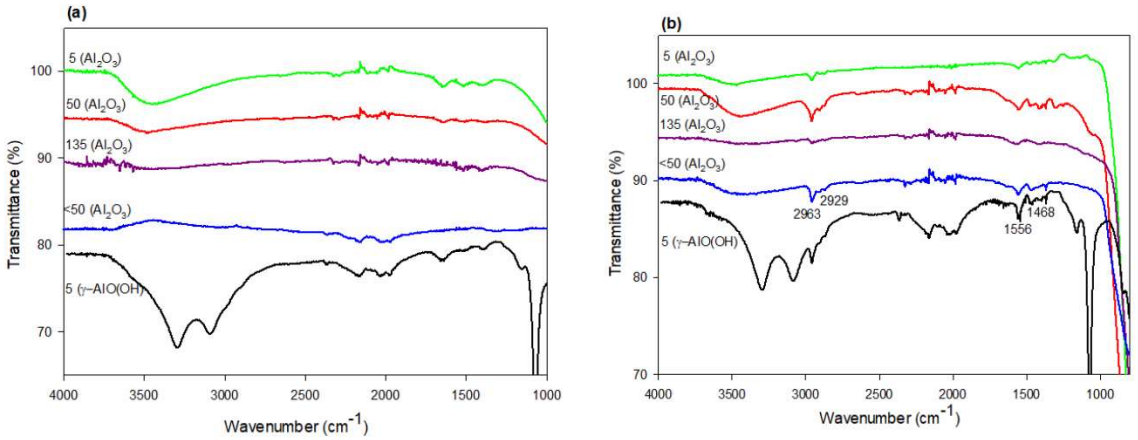

Fig. 1. ATR-IR spectra of the as received (a) and isostearic functionalized (b) nanoparticles.

TGA was performed on the as received nanoparticles and isosteaic functionalized nanoparticles (Fig. 2). This was conducted in order to calculate the acid grafting densities on

the surface of the nanoparticles. Weight losses of the as received nanoparticles were due to removal of surface hydroxyl groups and adsorbed H_2O mainly. It was observed that all of the nanoparticles showed more rapid weight loss between 50-200 °C ascribed to the removal of H_2O during heating (Fig. 2a). At temperatures greater than 200 °C weight losses are largely attributed to the removal of surface hydroxyl groups from the nanoparticles. The as received boehmite nanoparticles showed the largest weight loss between 200-800 °C, possibly because of their increased surface area and thus larger number of surface hydroxyl groups.

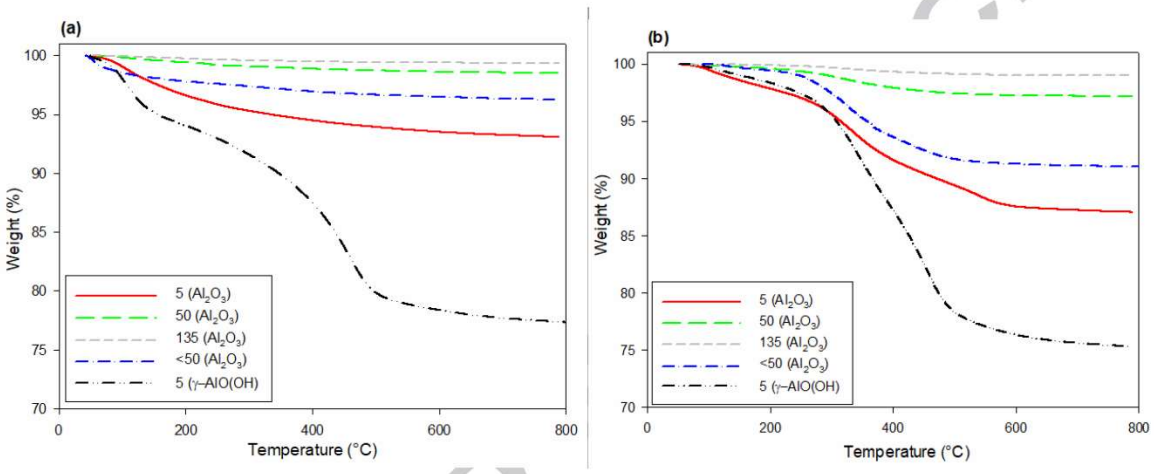

Fig. 2. TGA heating profiles of the as received (a) and isostearic functionalized (b) nanoparticles.

It was observed that the pure isostearic acid used in this study underwent combustion at approximately 200 °C [3]. By comparison, removal of chemisorbed isostearic from Al_2O_3 was observed to occur at temperatures greater than about 330 °C (Figure 2b). The organic weight losses listed in Table 2 are the differences between the mass losses observed in the heating profiles of the as received and functionalized nanoparticles. These values were used to calculate the acid grafting densities [3]. Using the TGA data, it was observed that the isostearic grafting densities of the spherical 5, 50, and 135 nm nanoparticles were ~1, 0.9 and 0.5 nm^{-2} respectively, which are consistent with the surface area of the nanoparticles. Notably (even by taking into consideration the NPs' specific surface area) these values are lower than the carboxylate grafting densities we have reported on spherical 13 nm Al_2O_3 particles, which were between 2-3 nm^{-2} [3], and also what other groups have reported in related studies [25,26]. These Al_2O_3 nanoparticles were purchased from a different manufacturer to what we have used previously, hence the lower grafting densities show that they are less reactive to what we have used in our previous syntheses.

TGA data also show that the mix shape 50 nm Al_2O_3 nanoparticles are substantially more reactive than the spherical Al_2O_3 particles studied here. The acid grafting density of these nanoparticles was calculated to be higher (by ~2.6 nm^{-2}), even more than to what we have observed in our previous studies [3,6]. This could suggest that carboxylic acids suffer less steric hindrance when they bind to mix shape (mainly cylindrical) nanoparticles, allowing more carboxylates to chemisorb onto the surface. The 5 nm boehmite nanoparticles were observed to have much lower carboxylic grafting density than the other nanoparticles, despite a larger amount of isostearic acid being used in the synthesis. This could suggest that 5 nm Al_2O_3 nanoparticles are more reactive to carboxylic acids than boehmite nanoparticles of the same size. Carboxylate functionalization of boehmite has been accomplished at higher temperatures in previous studies [27]. Consequently, it is possible that our reaction conditions were not vigorous enough to achieve a high carboxylate grafting density on this material.

Table 2.

TGA mass losses and isostearic grafting densities of the functionalized nanoparticles.

Type	Size (nm)	Weight loss of organic material (%)	Grafting density (nm^{-2})
Al_2O_3	5	6.4	1.0
Al_2O_3	50	1.4	0.9
Al_2O_3	135	0.4	0.5
Al_2O_3	<50	6.4	3.6
γ-AlO(OH)	5	6.4	0.6

3.2. Morphological investigations

SEM was performed on the nanoparticle films to visualize their morphological features. SEM showed that all of the Al_2O_3 nanoparticle films were composed of agglomerates of nanoparticles of various sizes (Fig. 3a-c). Cavities were observed between the nanoparticle agglomerates indicating that density variations exist within the films. As a consequence of the high degree of irregularity of the film structures it was difficult to determine whether the Al_2O_3 nanoparticle films were morphologically different. However, it was apparent that the unfunctionalized nanoparticle films (shown in Fig. S2 and S3) were less densely packed than analogous films created using the carboxylate functionalized nanoparticles. It is apparent from the Fig. 3c that the boehmite films have far fewer cavities between the surface features and also aggregates with various sizes (multi-components) are

formed compared to films formed by Al_2O_3 smaller nanoparticles which more monodisperse aggregates are observed.

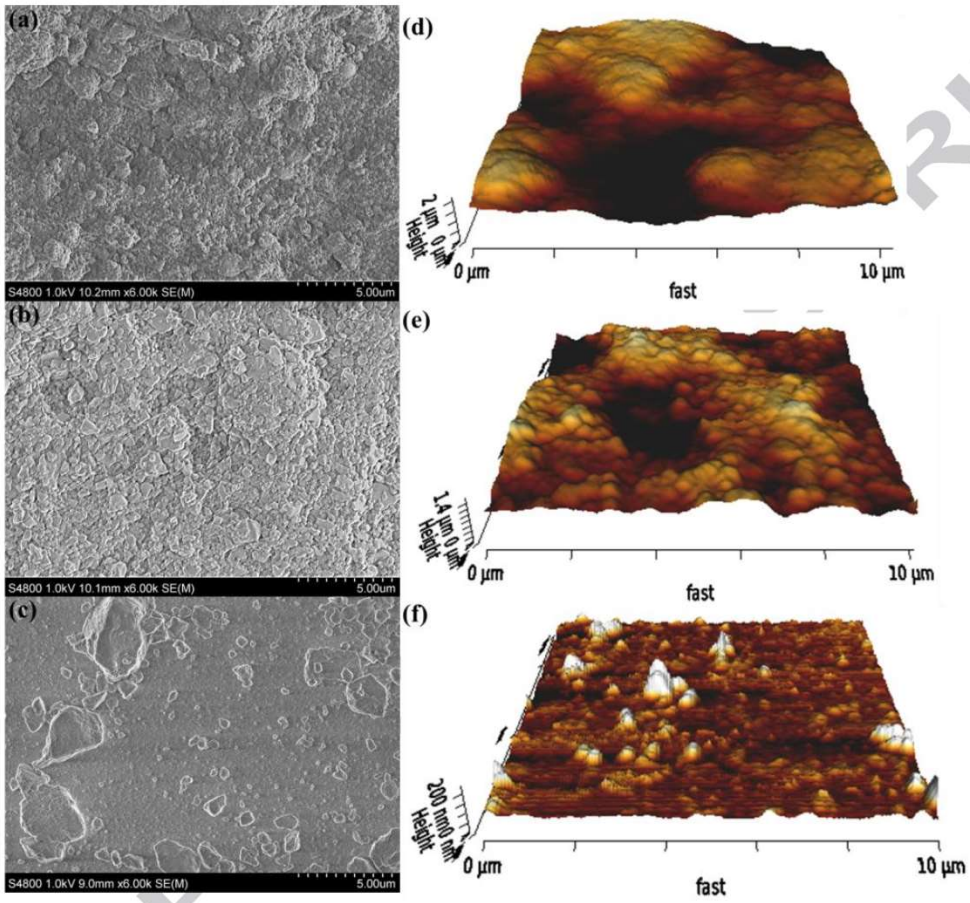

Fig. 3. SEM images of (a) isostearic functionalized 5 nm spherical Al_2O_3, (b) 135 nm spherical Al_2O_3, and (c) 5 nm boehmite nanoparticle films. AFM images of the isostearic (d) functionalized 5 nm spherical Al_2O_3, (e) 135 nm spherical Al_2O_3, and (f) 5 nm boehmite nanoparticle films.

AFM was used to study the roughness of the isostearic functionalized nanoparticle films. Table 3 shows the values of the surface roughness parameters of the different films. The large uncertainties associated with these values reflects the wide range of sizes of the different surface features. Despite this, useful information into the roughness of the films was obtained from the AFM images. It was observed that the spherical 5 and 50 nm nanoparticles created films that displayed the largest surface roughness parameters (Table 3). By comparison, the surface roughness parameters of the nanoparticle film formed from the 135 nm spherical Al_2O_3 nanoparticles were observed to be lower. These results are in line with

what has been observed for films formed from hydrophobic SiO_2 particles, where AFM showed that larger nanoparticles created films that displayed lower surface roughness [16].

Table 3

Surface roughness parameters of the isostearic-functionalized nanoparticle films.

Type	Size (nm)	Average roughness (R_a) (nm)	Root mean squared roughness (R_q) (nm)	Peak to valley roughness (R_t) (nm)
Al_2O_3	5	288 ±51	367 ±62	2325 ±382
Al_2O_3	50	414 ±144	496 ±165	3075 ±718
Al_2O_3	135	184 ±25	232 ±31	1599 ±43
Al_2O_3	<50	171 ±63	228 ±74	1792 ±625
γ-AlO(OH)	5	40 ±16	61 ±21	740 ±65

Interestingly, changing the shape of the nanoparticles affected large changes in the topography of the nanoparticle films. The 5 nm cubic boehmite nanoparticles generated a film that showed substantially reduced surface roughness, relative to when the 5 nm spherical Al_2O_3 nanoparticles were used (Table 3 and Fig. 3f). This could indicate that these nanoparticles pack together more effectively and generate more densely packed films. Similarly, the film formed from the mix shape 50 nm Al_2O_3 nanoparticles showed similar surface roughness parameters to the film created using the larger 135 nm Al_2O_3 nanoparticles, providing further evidence that spherical nanoparticles form rougher films.

Unfortunately, it was not possible to accurately measure the topography of films formed from the unfunctionalized nanoparticles. This was due to problems associated with nanoparticles moving around the surfaces during AFM measurements. This indicates that the unfunctionalized nanoparticles experience poorer adhesion with neighbouring particles in the films, suggesting that they are less densely packed relative to films prepared using the carboxylate-functionalized nanoparticles. Images showing packing variations between the as received and functionalized 135 nm Al_2O_3 nanoparticle films are displayed in Fig. S4.

3.3. Wetting properties of the nanoparticle films

As anticipated, chemisorption of isostearic acid onto the surface of the nanoparticles was observed to substantially increase the hydrophobicity of the nanoparticle films (Fig. 4). Prior to functionalization with isostearic acid, all of the films are hydrophilic (Table 1 and Fig. S5). WCAs of greater than 150° were observed for the films formed from the 5 and 50

nm spherical Al_2O_3 nanoparticles (Table 4 and Fig. 4), indicating that the roughness and grafting density of the isostearic chains was high enough to create superhydrophobic surfaces. Nevertheless, the WCA hysteresis for the film formed from the 5 nm spherical Al_2O_3 nanoparticles was substantially lower than the film composed of the 50 nm spherical Al_2O_3 nanoparticles (Table 4), indicating that the water droplets were less adherent and would more readily roll off the surface [9].

The WCA of the film formed from the 135 nm spherical Al_2O_3 nanoparticles was not superhydrophobic (Fig. 4) and possessed a larger hysteresis than the films from the smaller spherical particles. As discussed above, all of the spherical nanoparticles are functionalized with similar numbers of carboxylates. Consequently, the lower WCA and greater adhesion of the water droplets on the film formed from the 135 nm Al_2O_3 nanoparticles is more likely due to its lower roughness, in line with previous studies [16,19].

Interestingly, it was observed that the nanoparticle film formed from the mix shape < 50 nm Al_2O_3 nanoparticles displayed a WCA of greater than 150° (Table 4 and Figure 4), despite possessing similar roughness to the less hydrophobic film formed from the 135 nm Al_2O_3 nanoparticles. Since these nanoparticles were observed to be functionalized by the largest amount of isostearic acid this could suggest that topographical effects of the films could be overcome by greater carboxylate grafting densities. Furthermore, this film showed the lowest hysteresis out of all of the films studied, indicating the water droplets experience the lowest adhesive force when applied to this surface [9].

The film formed from the 5 nm cubic boehmite nanoparticles showed the lowest WCA (Table 4). This is perhaps unsurprising due to the low isostearic grafting density on the particles and smooth surface topography of the film (Fig. 3c and f). Using this data, it is not possible to ascertain whether the lower wettability is due to a topographical or chemical effect. However, WCAs of ~115° have been observed on carboxylate functionalized aluminium oxide films with low surface roughness [27], which could suggest that the more hydrophilic WCA of the boehmite film is due to its smoother topography.

Table 4.

Average contact angles and hysteresis values for the isostearic functionalized nanoparticle films.

Particle type	Size (nm)	Dynamic contact angle (°)					
		Advancing		Receding		Hysteresis	
		H_2O	CH_2I_2	H_2O	CH_2I_2	H_2O	CH_2I_2
Al_2O_3	5	153±2	57 ±2	144 ±1	49 ±1	9.0	8.0
Al_2O_3	50	158± 1	74 ±1	129 ±4	71 ±1	29.0	3.0
Al_2O_3	135	137 ± 4	70 ±2	80 ±3	65 ±2	51.0	5.0
Al_2O_3	<50	158 ± 3	101 ±2	151 ±3	84 ±4	7.0	17.0
γ-AlO(OH)	5	120±2	100 ±1	83 ±2	93 ±2	37.0	7.0

The wetting behaviour of diiodomethane droplets on the surfaces indicates that the nanoparticle films are oleophilic or slightly oleophobic (Table 4). This was anticipated since high levels of oleophobicity have largely been realized through functionalizing rough surface textures with species containing fluorocarbon groups [29-32]. Surfaces terminated with CF_3 groups have a lower surface energy than those terminated by CH_3 moieties [30,32]. Consequently, liquids with lower surface tensions than water, such as oils or iodomethane, show reduced wettability when applied to fluoro- as opposed hydrocarbon-functionalized surfaces [30-32]. As is shown in Fig. 4, chemisorption of isostearic onto the nanoparticles reduces their surface energy, relative to the values provided in Table 1. Films formed from the mix shape < 50 nm Al_2O_3 nanoparticles and 5 nm boehmite nanoparticles showed the lowest surface energy out of all the films. This is due to a larger contribution to the surface energy from the dispersive (CH_2I_2) component.

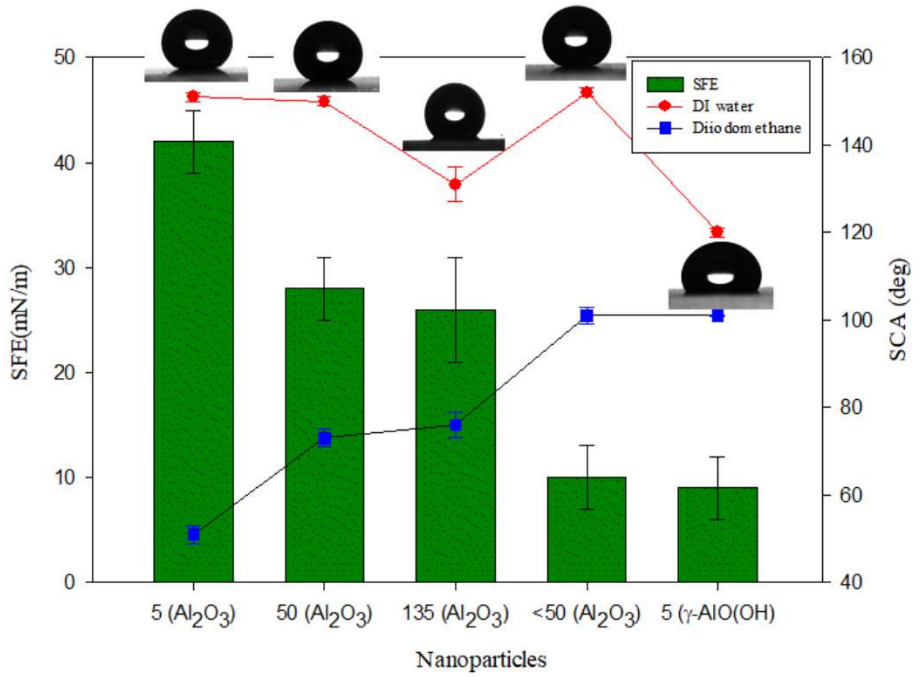

Fig. 4. Plot of the static contact angles (SCAs) of H_2O and diiodomethane droplets of the different nanoparticle films and their surface free energy (SFE). Images of 4 µL water droplets on the appropriate surface are also shown.

4. Conclusions

While it has shown previously that certain metal oxide nanoparticles can create hydrophobic surfaces [1-6], this work investigates a number of important factors that influence the wettability of carboxylate functionalized aluminium oxide nanoparticle films. We show that although roughness and chemical functionality are essential for tuning the hydrophobicity, nevertheless the size, shape, and reactivity of the nanoparticles also play significant roles when designing suitable hydrophobic surfaces. Spherical particles, with sizes of <50 nm, were observed to create rougher films and display superhydrophobic properties. Consequently, they are well suited to be used as scaffolds to create low wettability coatings. Larger spherical aluminium oxide nanoparticles, which are at least 135 nm in size, generate films with lower surface roughness, making them less useful for fabricating superhydrophobic coatings.

This study also demonstrates that nanoparticle shape in addition to size plays an important role. Although nanoparticles with non-spherical morphologies created films that showed reduced surface roughness, the highest WCA and lowest hysteresis was observed for a film created using mix shape nanoparticles. TGA revealed that these nanoparticles

possessed a substantially higher carboxylate grafting density than the spherical particles studied here and previously [3,6], indicating that the mix shape particles were more reactive towards chemisorption of carboxylic acids. This specifies that topographical effects caused by lower film roughness can be overcome by using nanoparticles that show a greater extent of functionalization. In summary, when selecting nanoparticles for creating low wettability coatings it is important to consider nanoparticles on the basis of their shape, in addition to their size. This work could be beneficial for users who wish to develop low surface energy surfaces based on metal oxide nanoparticles, since it widens the specification of particles that could be used in the application.

Acknowledgment

Financial support was provided by the Welsh Government Sêr Cymru Programme through Sêr Cymru II Welsh Fellowship part funded by the European Regional Development Fund (ERDF) (S.A.) and the Sêr Cymru Chair for Low Carbon Energy and Environment (A.R.B.). The Robert A.Welch Foundation (C-0002) is acknowledged for additional support (A.R.B.). H.A. would like to thank the Ministry of Higher Education and Scientific Research/Iraq and Al-Mustansiriya University/Baghdad for providing PhD scholarship.

Appendix A. Supplementary material

Supplementary data associated with this article can be found, in the online version. SEM/TEM images of the as received nanoparticles, SEM and AFM images of the unfunctionalized and functionalized nanoparticles.

References

[1] Y. Gao, I. Gereige, A. El Labban, D. Cha, T.T. Isimjan, P. M. Beaujuge, Highly transparent and UV-resistant superhydrophobic SiO_2-coated ZnO nanorod arrays, ACS Appl. Mater. Interfaces 6 (2014) 2219-2223.

[2] X.-M. Bao, J.-F. Cui, H.-X. Sun, W.-D. Liang, Z.-Q. Zhu, J. An, B.-P. Yang, P.-Q. La, A. Li, Facile preparation of superhydrophobic surfaces based on metal oxide nanoparticles, Appl. Surf. Sci. 303 (2014) 473-480.

[3] S. Alexander, J. Eastoe, A.M. Lord, F. Guittard, A.R. Barron, Branched hydrocarbon low surface energy materials for superhydrophobic nanoparticle derived surfaces, ACS Appl. Mater. Interfaces 8 (2016) 660-666.

[4] N. Agrawal, S. Munjal, M. Z. Ansari, N. Khare, Superhydrophobic palmitic acid modified ZnO nanoparticles, Ceram. Int. 43 (2017) 14271-14276.

[5] Z.-T. Li, B. Lin, L.-W. Jiang, E.-C. Lin, J. Chen, S.-J. Zhang, Y.-W. Tang, F.-A. He, D.-H. Li, Effective preparation of magnetic superhydrophobic Fe_3O_4/PU sponge for oil-water separation, Appl. Surf. Sci. 427 (2018) 56-64.

[6] W. Al Shatty, A.M. Lord, S. Alexander, A.R. Barron, Tunable surface properties of aluminum oxide nanoparticles from highly hydrophobic to highly hydrophilic, ACS Omega 2 (2017) 2507-2514.

[7] Z. Guo, W. Liu, B.- Lian Su, Superhydrophobic surfaces: From natural to biomimetic to functional, J. Colloid Interface Sci. 353 (2011) 335-355.

[8] E. Celia, T. Darmanin, E. T. de Givenchy, S. Amigoni, F. Guittard, Recent advances in designing superhydrophobic surfaces, J. Colloid Interface Sci. 402 (2013) 1-18.

[9] G. McHale, N. J. Shirtcliffe, M. I. Newton, Contact-Angle Hysteresis on Super-Hydrophobic Surfaces, Langmuir 20 (2004) 10146-10149.

[10] R. Liao, Z. Zuo, C. Guo, Y. Yuan, A. Zhuang, Fabrication of superhydrophobic surface on aluminum by continuous chemical etching and its anti-icing property, Appl. Surf. Sci. 317 (2014) 701-709.

[11] D. K. Sarkar, M. Farzaneh, R. W. Paynter, Superhydrophobic properties of ultrathin rf-sputtered Teflon films coated etched aluminum surfaces, Mater. Lett. 62 (2008) 1226-1229.

[12] J. Yong, Y. Fang, F. Chen, J. Huo, Q. Yang, H. Bian, G. Du, X. Hou, Femtosecond laser ablated durable superhydrophobic PTFE films with micro-through-holes for oil/water separation: Separating oil from water and corrosive solutions, Appl. Surf. Sci. 389 (2016) 1148-1155.

[13] D. V. Ta, A. Dunn, T. J. Wasley, R. W. Kay, J. Stringer, P. J. Smith, C. Connaughton, J. D. Shephard, Nanosecond laser textured superhydrophobic metallic surfaces and their chemical sensing applications, Appl. Surf. Sci. 357 (2015) 248-254.

[14] K. Tsougeni, N. Vourdas, A. Tserepi, E. Gogolides, Mechanisms of Oxygen Plasma Nanotexturing of Organic Polymer Surfaces: From Stable Super Hydrophilic to Super Hydrophobic Surfaces, Langmuir 25 (2009) 11748-11759.

[15] K. Tsougeni, A. Tserepi, G. Boulousis, V. Constantoudis, E. Gogolides, Control of Nanotexture and Wetting Properties of Polydimethylsiloxane from Very Hydrophobic to Super-Hydrophobic by Plasma Processing, Plasma Processes Polym. 4 (2007) 398-405.

[16] R. G. Karunakaran, C.- H. Lu, Z. Zhang, S. Yang, Highly Transparent Superhydrophobic Surfaces from the Coassembly of Nanoparticles (<100 nm), Langmuir 27 (2011) 4594-4602.

[17] J. Bravo, L. Zhai, Z. Wu, R. E. Cohen, M. F. Rubner, Transparent Superhydrophobic Films Based on Silica Nanoparticles, Langmuir 23 (2007) 7293-7298.

[18] 18. L. Cao, A. K. Jones, V. K. Sikka, J. Wu, Di Gao, Anti-Icing Superhydrophobic Coatings, Langmuir 25 (2009)12444-12448.

[19] M. Miwa, A. Nakajima, A. Fujishima, K. Hashimoto, T. Watanabe, Effects of the Surface Roughness on Sliding Angles of Water Droplets on Superhydrophobic Surfaces, Langmuir 16 (2000) 5754-5760.

[20] https://www.kruss-scientific.com.

[21] Le´dion, G. Sattonnay, J. B. Brubach, P. Berthet, A. M. Huntz, P. o ç ó Te´tot, Transition alumina phases induced by heat treatment of boehmite: An X-ray diffraction and infrared spectroscopy study, J. Solid State Chem. 182 (2009) 1171-1176.

[22] R. R. Sahoo, S. K. Biswas, Frictional response to fatty acids on steel, J. Colloid Interface Sci. 333 (2009) 707-718.

[23] Q. Zhang, Y. Wan, Y. Li, S. Yang, W. Yao, Friction reducing behavior of stearic acid film on a textured aluminum substrate, Appl. Surf. Sci. 280 (2013) 545-549.

[24] A. D. Roddick-Lanzilotta, A. J. McQuillan, An in situ Infrared Spectroscopic Study of Glutamic Acid and of Aspartic Acid Adsorbed on TiO_2: Implications for the Biocompatibility of Titanium, J. Colloid Interface Sci. 227 (2000) 48-54.

[25] H. Klauk, U. Zschieschang, J. Pflaum, Marcus Halik, Ultralow-power organic complementary circuits, Nat. Let. 445 (2007) 745-748.

[26] S. Anaya, B. Serrano, B. Herrero, A. Cervera, J. Baselga, γ-Alumina Modification with Long Chain Carboxylic Acid Surface Nanocrystals for Biocompatible Polysulfone Nanocomposites, ACS Appl. Mater. Interfaces 6 (2014) 14460-14468.

[27] Y. Koide, A. R. Barron, $[Al_5(^tBu)_5(\mu_3\text{-}O)_2(\mu_3\text{-}OH)_3(\mu\text{-}OH)_2(\mu\text{-}O_2CPh)_2]$: A Model for the Interaction of Carboxylic Acids with Boehmite. *Organomet.* 14 (1995) 4026-4029.

[28] T. T. Foster, M. R. Alexander, G. J. Leggett, E. McAlpine, Friction Force Microscopy of Alkylphosphonic Acid and Carboxylic Acids Adsorbed on the Native Oxide of Aluminum, Langmuir 22 (2006) 9254-9259.

[29] H. J, Lee, J. R. Owens, Motion of liquid droplets on a superhydrophobic oleophobic surface, J. Mater. Sci. 46 (2011) 69-76.

[30] J. Yong, F. Chen, Qing Yang, J. Huo, X. Hou, Superoleophobic surfaces, Chem. Soc. Rev. 46 (2017) 4168-4217.

[31] T. Darmanin, F. Guittard, Fluorophobic Effect for Building up the Surface Morphology of Electrodeposited Substituted Conductive Polymers, Langmuir 25 (2009) 5463-5466.

[32] Z. Xue, M. Liu, Lei Jiang, Recent Developments in Polymeric Superoleophobic, J. Polym. Sci., Part B: Polym. Phys. 50 (2012) 1209-1224.

Electronic Supporting Information (ESI)

Size and Morphology Dependent Surface Wetting Based on Hydrocarbon Functionalized Nanoparticles

Donald Hill,[a] *Hadi Attia,*[b,c] *Andrew R. Barron,*[a,d,e] *Shirin Alexander*[*a]

[a] Energy Safety Research Institute (ESRI), Swansea University Bay Campus, Fabian Way, Swansea SA1 8EN, UK.

[b] Centre for Water Advanced Technologies and Environmental Research (CWATER), College of Engineering, Swansea University, Fabian Way, Swansea SA1 8EN, UK.

[c] Environmental Engineering Department, Al-Mustansiriya University, Iraq

[d] Department of Chemistry, Rice University, Houston, TX 77005, USA.

[e] Department of Materials Science and Nanoengineering, Rice University, Houston, Texas 77005, USA.

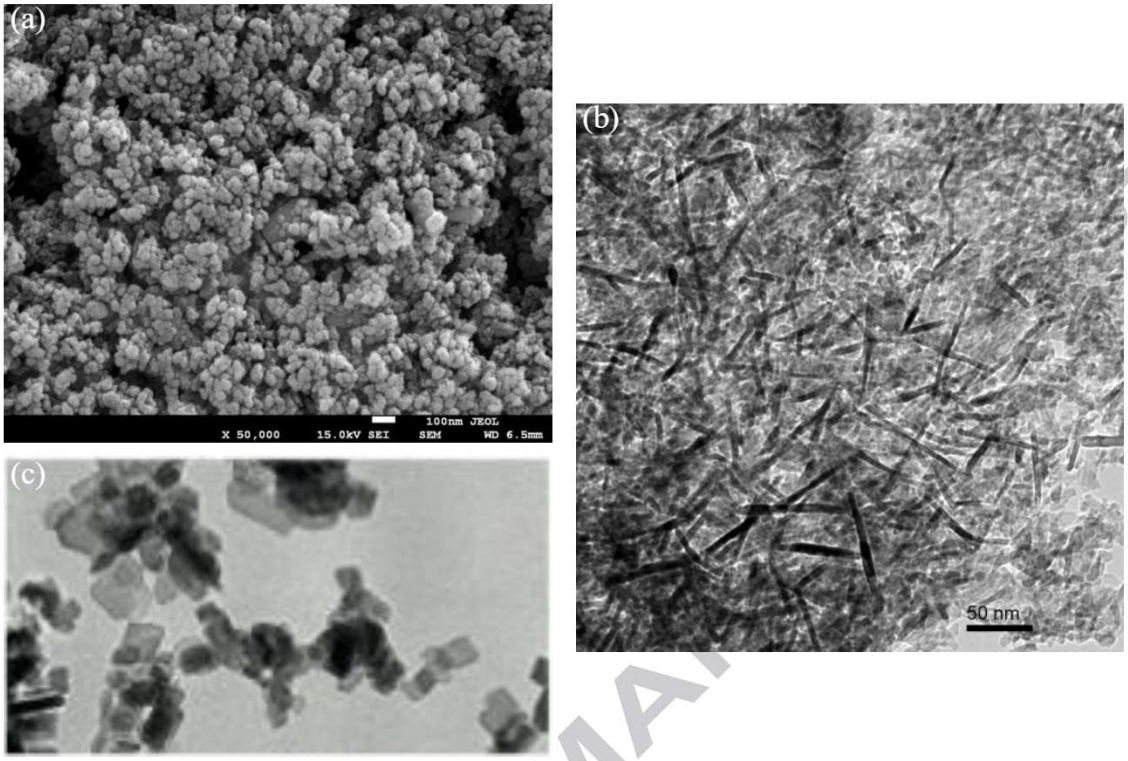

Fig. S1. SEM image of the 50 nm spherical Al_2O_3 nanoparticles (a) (www.us-nano.com), and TEM images of the 50 nm mix shape Al_2O_3 nanoparticles (www.sigmaaldrich.com) and the 5 nm cubic pseudo-boehmite nanoparticles (c) (http://sasolnorthamerica.com). The images are taken from the manufacturer's websites.

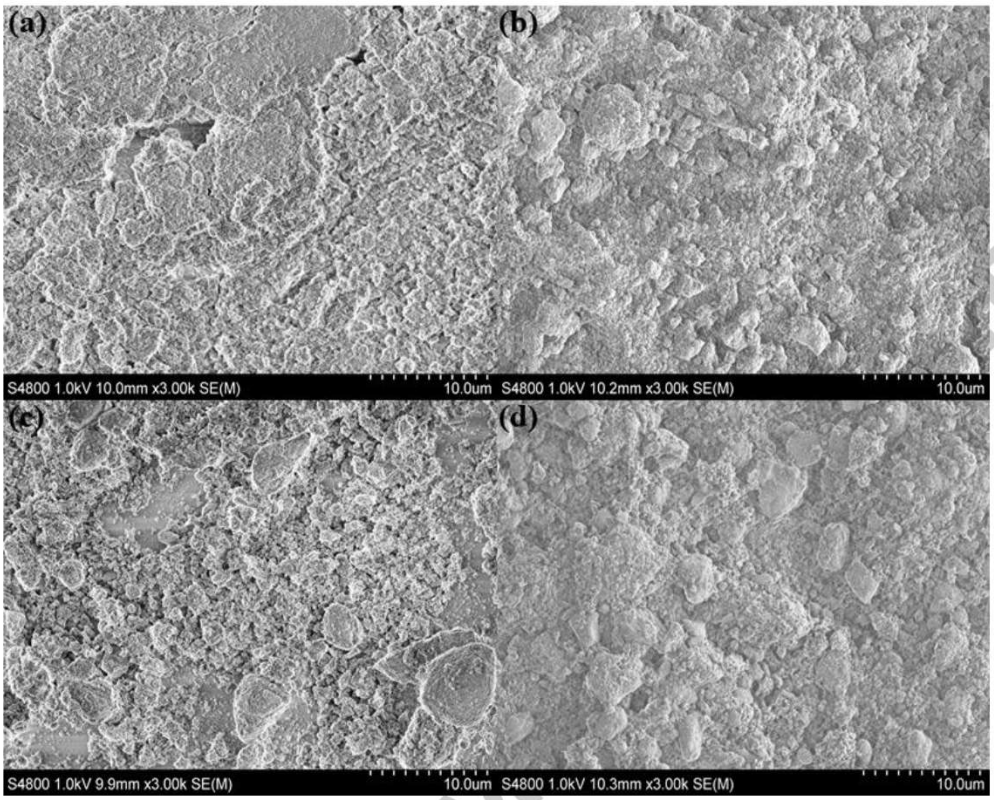

Fig. S2. SEM images of the as received spherical 5nm Al_2O_3 nanoparticle film (a), the isostearate functionalized spherical 5nm Al_2O_3 nanoparticle film (b), the as received spherical 50nm Al_2O_3 nanoparticle film (c), and the isostearate functionalized spherical 50nm Al_2O_3 nanoparticle film.

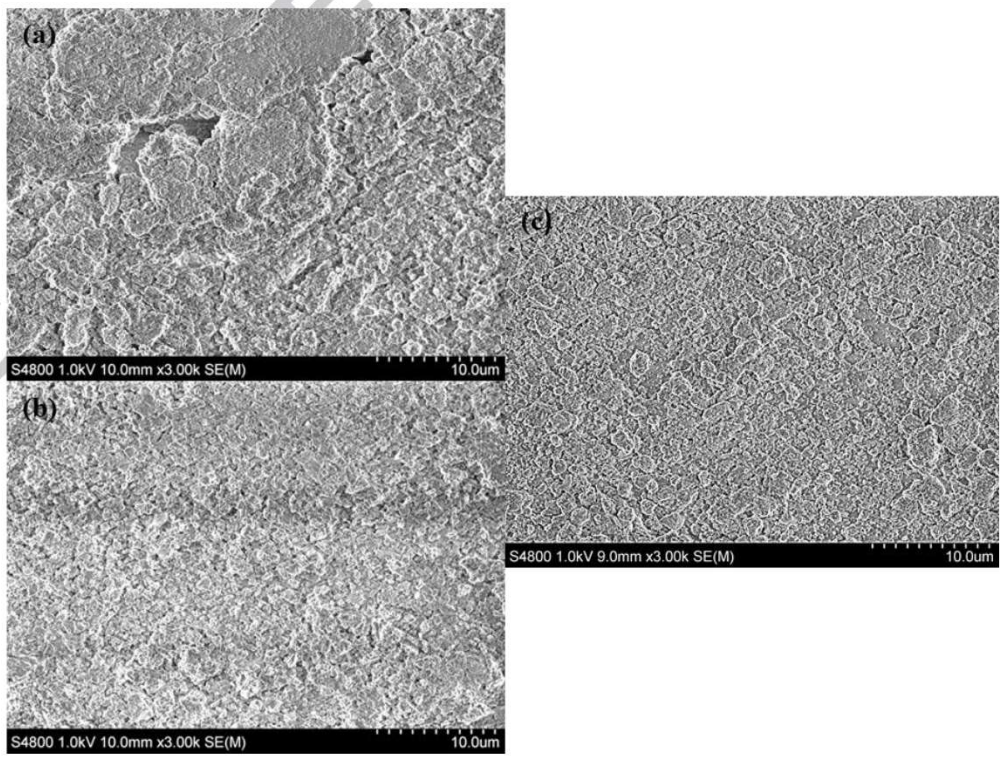

Fig. S3. SEM images of the as received nanoparticle film (a) 5 nm bohemite, (b) 50 nm mix shape, and (c) 135 nm spherical nanoparticle.

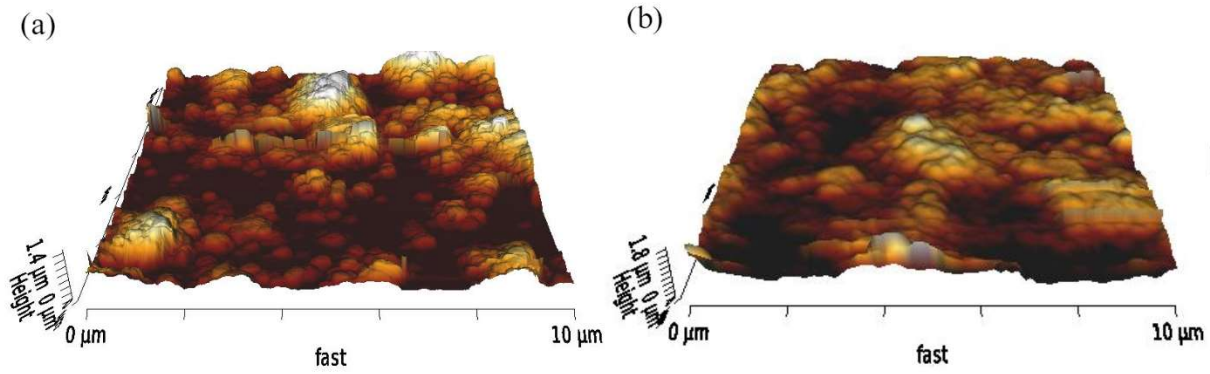

Figure S4. AFM images of films created using the as received (a) and isostearate functionalized 135 nm Al_2O_3 nanoparticles (b).

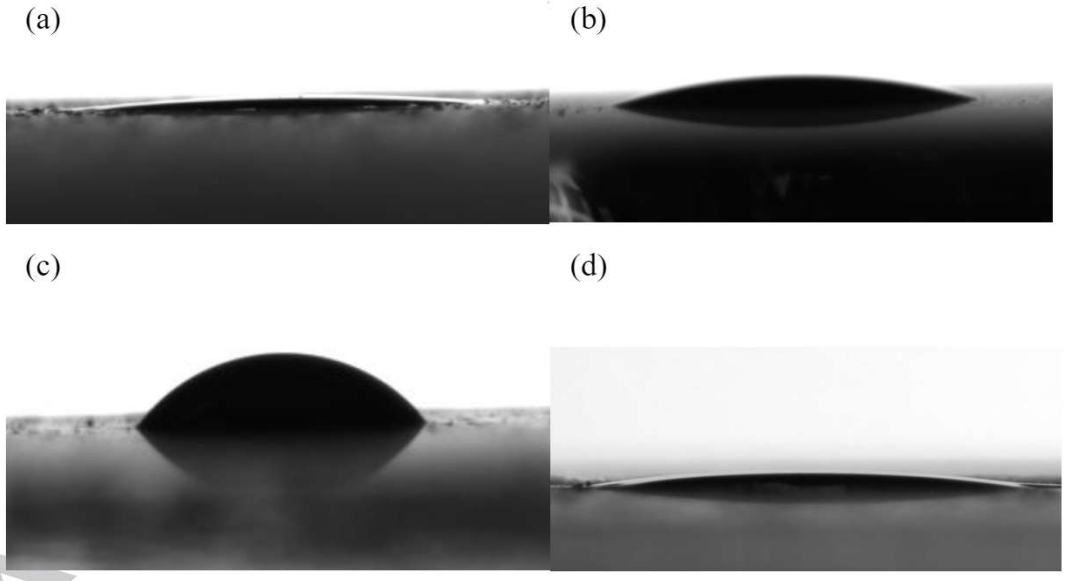

Fig. S5. Images of 4 µl water droplets on the as received nanoparticle films (a) 5 nm spherical Al_2O_3, (b) 50 nm spherical , (c) 135 nm spherical, and (d) 5 nm boehmite nanoparticle.